

Microscopic Binding of M5 Muscarinic Acetylcholine Receptor with Antagonists by Homology Modeling, Molecular Docking, and Molecular Dynamics Simulation

Xiaoqin Huang,[†] Guangrong Zheng,[‡] and Chang-Guo Zhan^{*,†}

[†]Department of Pharmaceutical Sciences, College of Pharmacy, University of Kentucky, 789 South Limestone Street, Lexington, Kentucky 40536, United States

[†]Department of Pharmaceutical Sciences, College of Pharmacy, University of Arkansas for Medicinal Sciences, 4301 West Markham Street, Little Rock, Arkansas 72205, United States

S Supporting Information

ABSTRACT: By performing homology modeling, molecular docking, and molecular dynamics (MD) simulations, we have developed three-dimensional (3D) structural models of the M5 muscarinic acetylcholine receptor (mAChR) and two complexes for M5 mAChR binding with antagonists SVT-40776 and solifenacin in the environment of lipid bilayer and solvent water. According to the simulated results, each of the antagonists is oriented horizontally in the binding pocket formed by transmembrane helices 2, 3, and 5–7. The cationic headgroup of each of the antagonists interacts with a negatively charged residue, Asp110, through electrostatic and hydrogen-bonding interactions. The simulated results also reveal some significant difference between the binding modes of SVT-40776 and solifenacin. In particular, SVT-40776 is persistently hydrogen bonded with the side chain of residue Tyr458, whereas solifenacin cannot form a similar hydrogen bond with residues around its carbonyl group. Such significant difference in the binding structures is consistent with the fact that SVT-40776 has a much higher binding affinity ($K_d = 0.4$ nM) to M5 mAChR than that of solifenacin ($K_d = 31$ nM) with the same receptor. The calculated binding free energy change (-2.3 ± 0.5 kcal/mol) from solifenacin to SVT-40776 is in good agreement with the experimentally derived binding free energy change (-2.58 kcal/mol), suggesting that our modeled M5 mAChR structure and its complexes with the antagonists are reliable. The new structural insights obtained from this computational study are expected to stimulate further biochemical and pharmacological studies on the detailed structures of M5 and other subtypes of mAChRs.

■ INTRODUCTION

The muscarinic acetylcholine receptors (mAChRs) mediate many actions of neurotransmitter acetylcholine in the central and peripheral nervous systems. These receptors have been found to play very important and diverse roles in many physiological processes such as cardiovascular, motor, attention, learning, memory, pain, and sleep.¹⁻⁴ Different from the nicotinic acetylcholine receptors (nAChRs), which are ligand-gated ion channels formed by five subunits, mAChRs are G-protein-coupled receptors (GPCRs), which operate through G-proteins to alter second messenger systems involving adenylate cyclase and phospholipase C β . The mAChRs belong to the class-A GPCRs and have five distinct subtypes (M1 to M5). The M5 mAChR is expressed primarily at the substantia nigra, ventral tegmental area, cerebral cortex, and striatum area of the central nervous system (CNS).^{1,2} Recent studies revealed that M5 mAChR was involved in the regulation of striatal dopamine release and in rewarding brain stimulations.⁵⁻⁷ It was also found that M5 mAChR-knockout mice had reduced morphine-induced locomotion, establishing that M5 mAChR is a potential target for the

treatment of drug abuse.^{8–11} Therefore, it has become a high priority to understand the molecular mechanisms for M5 mAChR agonist and antagonist processes, and develop novel and selective M5 ligands as potential therapeutics.

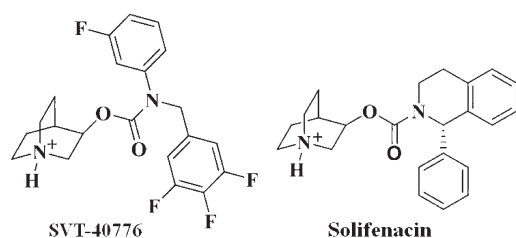
The first highly potent ligand of M5 mAChR was derived from a series of 5-trifluoromethoxy *N*-benzyl isatins and found to be a positive allosteric modulator.¹² Some other compounds were also developed to be high-affinity antagonists of mAChRs, but these compounds did not show significant selectivity toward the M5 receptor.^{13–16} To design highly potent and M5 mAChR-selective agonists or antagonists, one needs to understand the molecular determinants for the M5 mAChR–ligand binding and then perform structure-based ligand design. For this purpose, one first needs to develop a reasonable and reliable structural model of M5 mAChR–ligand complex. Because of the difficulty in protein expression and crystallization of membrane proteins,

Received: September 2, 2011

Revised: November 30, 2011

Published: December 20, 2011

Scheme 1



there is no available high-resolution crystal structure for any subtype of mAChR from any species. However, recent progress in structure–function studies on mAChRs and some other class-A GPCRs have paved the way to fully understanding the structure–function relationships of mAChRs.^{11,17–21} For example, the X-ray crystal structures for different conformational states of rhodopsin^{22–24} from different species have provided fundamental insights into the molecular details on the receptor activation mechanism. High-resolution X-ray crystal structures of human β_2 adrenergic receptor^{25–27} bound with an inverse agonist revealed significant structural difference for both the transmembrane helices and the second extracellular loop (EL-2) when compared with the structures of rhodopsin. The crystal structure of turkey β_1 adrenergic receptor (β_1 -AR)²⁸ bound with high-affinity antagonist represents a possible extracellular open conformational state for the adrenergic receptors. In this X-ray structure of β_1 -AR, the antagonist cyanopindolol (CYP) was located inside a binding pocket formed by transmembrane (TM) helices 3 and 5–7. The *tert*-butylamino group (cationic head) of CYP interacted with the negatively charged side chain of residue Asp121 from TM3 of β_1 -AR through both electrostatic and hydrogen-bonding interactions. The crystal structure of human A_{2A} adenosine receptor²⁹ bound with the selective antagonist demonstrated that the EL-2 and the antagonist binding site of adenosine receptors are quite different from those of rhodopsin and the adrenergic receptors. The differences in receptor structures and the ligand-binding sites observed from these crystal structures indicate that each subfamily of GPCRs may have different inherent structural flexibility and, therefore, adopt different conformational states under different incoming stresses. The latest information from the X-ray crystal structures for CXCR4 receptor³⁰ bound with antagonists further support the viewpoint about the structural flexibility and functional diversity of GPCRs. This background indicates that it is a challenge to reliably study the structural mechanisms for other GPCRs. Special attention needs to be paid to the selection of a template for the construction of a structural model of any other specific GPCR. For the available X-ray structures of bovine rhodopsin, the native agonist (i.e., retinal) is covalently bound with the side chain of residue Lys296 of the receptor. The sequence identity between bovine rhodopsin and mAChRs is quite low (mostly <20%). Thus, the structure of bovine rhodopsin is not a suitable template for use in homology modeling of mAChR binding with antagonists. Earlier homology models of mAChRs based on the X-ray structure of bovine rhodopsin did not account for the possible difference at the ligand binding site.^{31–34} Thus, the modeled atomic contacts between the mAChR and ligand are not reliable. Phylogenetically, mAChRs are more closely related to adrenergic receptors than either adenosine receptors or the CXCR4 receptor.^{17,23} Currently, the antagonist-bound β_1 -AR

is the most reasonable and appropriate template to model the structures of mAChRs for the purpose of studying the receptor–antagonist binding. The combined use of the X-ray structure of β_1 -AR–antagonist complex and current computational modeling has enabled us to construct a reasonable 3D model of M5 mAChR.

The present study aimed to develop a reasonable structural model of M5 mAChR and its binding with antagonists. For this purpose, the 3D structure of human M5 mAChR was modeled, focusing on its binding with two representative antagonists (Scheme 1), (R)-quinuclidin-3-yl 3-fluorophenyl(3,4,5-trifluorobenzyl)carbamate (SVT-40776) and (1S,3'R)-quinuclidin-3'-yl 1-phenyl-1,2,3,4-tetrahydroisoquinoline-2-carboxylate (solifenacin).^{13,15} On the basis of the energy-minimized structure of M5 mAChR, the protonated species of these two antagonists were docked into the binding site. The intermolecular interactions between M5 mAChR and the antagonists were analyzed based on the trajectories of subsequent molecular dynamics (MD) simulations. We found that SVT-40776 can form an additional hydrogen bond with the side chain of residue Tyr458 of M5 mAChR, which is consistent with the fact that SVT-40776 has an affinity higher than that of solifenacin with the same receptor. The new structural insights obtained from this computational study should be valuable for further biochemical and pharmacological studies on M5 and other subtypes of mAChRs.

COMPUTATIONAL METHODS

Homology Modeling and Structural Optimization. To study the binding of SVT-40776 and solifenacin with M5 mAChR in atomic detail, a homology model of human M5 mAChR was built based on the X-ray crystal structure of turkey β_1 -AR (PDB entry 2VT4 at 2.7 Å resolution, B chain)²⁸ by using the Protein Modeling module of Discovery Studio (version 2.5.5, Accelrys, Inc., San Diego, CA). The amino acid sequence of human M5 mAChR was directly extracted from the uniprot.org (access number: P08912). The sequence alignment was generated by using ClusterW with the Blosum scoring function.^{35,36} The best alignment was selected according to both the alignment score and the reciprocal positions of the conserved residues among all the subtypes of mAChRs and adrenergic receptors. These include the DRY motif near the intracellular end of transmembrane 3 (TM3), the NPxxY(x)₆F motif from TM7, and the position of the disulfide bond between the Cys103 near the extracellular end of TM3 and the Cys183 of EL-2. The first 27 residues at the N-terminus, the last 20 residues at the C-terminus, and the third intracellular loop (IL-3, residues 225–435) of M5 mAChR were omitted because of the lack of a corresponding homologue sequence in the template. The alignment was first performed by using the default values of the parameters in program ClusterW,³⁵ e.g., the minimum sequence length of aligning was set as 10 and then was improved by adjusting the values of the parameters to obtain a higher alignment score. During the alignment process, the most important conserved motifs (i.e., the DRY motif from TM3, and the NPxxY(x)₆F motif from TM7) were strictly reserved from the previous round of alignment to the next round of alignment, while the newly aligned conserved regions were also added for further alignment. The sequence identity for the regions except the omitted ones reached 34.3%, and the sequence homology became 61.7% for the final alignment with 277 residues of β_1 -AR. We also tried to use another scoring function, i.e., the PAM matrix.³⁵ According to the

sequence alignment based on the PAM matrix, the sequence identity was 31.2%, lower than that for the sequence alignment based on the Blosom scoring function. The use of the PAM matrix could not align the conserved residue Cys183 of M5 mAChR with Cys199 of β_1 -AR. On the basis of the criteria of sequence identity and the reciprocal positions of the conserved residues, we finally elected to use the sequence alignment generated by using the Blosom scoring function. The coordinates of the heavy atoms in the conserved regions were directly transformed from the template structure (i.e., the X-ray crystal structure of β_1 -AR²⁸), whereas the nonequivalent residues were mutated from the template to the corresponding ones of M5 mAChR. The side chains of the nonconserved residues were relaxed during the process of homology modeling to remove the possible steric overlap or hindrance with the neighboring conserved residues.

To simulate the actual physiological environment, the initial M5 mAChR model was inserted into a pre-equilibrated POPC lipid bilayer and then solvated by two layers of water molecules at each side of the lipid bilayer. The area per lipid (A_L) for this starting lipid bilayer was calculated as the area of the xy plane of the simulation box divided by the number of lipid molecules per layer. The all-atom model of the POPC bilayer was generated by using the membrane plug-in of the VDW software,³⁷ and the initial size of the membrane was expanded to be large enough to encompass the target protein. The geometry of the POPC molecule was optimized by performing ab initio electronic structure calculation at the HF/6-31G* level using the Gaussian03 program.³⁸ The HF/6-31G* calculation was also performed to determine the restrained electrostatic potential (RESP)-fitted charges for POPC molecules. The relative orientation of M5 mAChR in the lipid bilayer was determined by referring to a similar orientation of the β_1 -AR structure,²⁸ i.e., the helix 8 in parallel with the intracellular surface of the membrane. When inserted, any POPC molecule was removed if it had more than 50% of its non-hydrogen atoms within a distance of 2.5 Å to any non-hydrogen atoms of M5 mAChR. The solvent layers were added by using the LEaP module of the Amber11 program suite.³⁹ The protein together with the lipid bilayer was solvated in a rectangular box of TIP3P water molecules⁴⁰ with a minimum solute wall distance of 10 Å. Standard protonation states at physiological environment (pH \sim 7.4) were set to all ionizable residues of M5 mAChR, and the position of the proton was properly set on the N δ 1 atom of residue His478. An additional 11 Cl[−] ions were added to the solvent as counterions to neutralize the system. The system was composed of 42 911 atoms, including 132 POPC molecules and 6892 water molecules.

After the whole system was set up, a series of energy minimizations (geometric optimizations) were carried out by using the Sander module of the Amber11 program suite³⁹ using the conjugate gradient energy-minimization method with a nonbonded cutoff of 10 Å. The first 2000 steps of the energy minimization was done for the backbone of M5 mAChR while the side chains were fixed, and then the next 40 000 steps for the lipid molecules, water molecules, and the side-chain atoms of M5 mAChR. To get the solute (M5 mAChR) better solvated, the subsequent MD simulations and energy minimizations were performed on the environment (i.e., the lipid molecules, water molecules, and the counterions). First, 1.0 ns MD simulations were performed on the water molecules with the NTV ensemble at $T = 300$ K. The environment was energy-minimized for 20 000 steps followed by a 2.0 ns MD simulation on the lipid molecules

with anisotropic pressure coupling (i.e., the parameter ntp = 2 in the input file). After these MD simulations, the environment and side chains of M5 mAChR were energy-minimized for 20 000 steps. Finally, the system was energy-minimized for 6000 steps for all atoms, and a convergence criterion of 0.001 kcal mol^{−1} Å^{−1} was achieved.

Molecular Docking and MD Simulation. On the basis of the structural model of M5 mAChR obtained in the present study, the binding modes of the receptor with two antagonists (Scheme 1) were explored through molecular docking by using the AutoDock 3.0.5 program.⁴¹ Previous site-directed mutation on Asp105 of M1 mAChR and mutation on Asp103 of M2 mAChR¹¹ showed that these negatively charged residues are critical for the ligand binding. This negatively charged residue from TM3 of the M1 or M2 receptor corresponds to residue Asp121 from TM3 of β_1 -AR²⁸ and to residue Asp110 of M5 mAChR. On the basis of the sequence comparison between M5 mAChR and β_1 -AR, and on the basis of the fact that both SVT-40776 and solifenacin are competitive antagonists,^{13,15} it is reasonable to assume that the binding site of M5 mAChR for these typical antagonists should be around residue Asp110 from TM3. The atomic charges of the protonated antagonists were also determined as the restrained electrostatic potential (RESP) charges determined by using the standard RESP procedure implemented in the Antechamber module of the Amber11 program³⁹ following the electronic structure and electrostatic potential calculations at the HF/6-31G* level. During the docking process, a conformational search was performed using the Solis and Wets local search method,⁴² and the Lamarckian genetic algorithm (LGA)⁴¹ was applied to deal with the M5 mAChR–antagonist interactions. Among a series of docking parameters, the grid size was set to be 60 \times 60 \times 60 and the grid space was the default value of 0.375 Å. The possible binding site of M5 mAChR for these two antagonists was first roughly defined as a site similar to that of the β_1 -AR structure for the antagonist cyanopindolol,²⁸ i.e., the cavity around transmembrane helices 2, 3, and 5–7. The binding site was then hunted by changing the center and the size of the docking grid. All the complex candidates were evaluated and ranked in terms of the binding energy by using the standard energy score function implemented in the docking program and, finally, the geometric matching quality through visual checking. For each antagonist, the initial binding structure was selected from the docked candidates, of which the protonated headgroup (Scheme 1) was oriented toward the negatively charged side chain of Asp110 of M5 mAChR. The selected initial structure of M5 mAChR–SVT-40776 complex was ranked no. 1 in the clustering histogram, with a positional root-mean square deviation (rmsd) of 1.63 Å from the average structure of the same cluster. The selected initial structure of M5 mAChR–solifenacin complex was also ranked no. 1 in clustering histogram, with an rmsd value of 0.80 Å.

To further relax the selected initial M5 mAChR–antagonist complex structures, MD simulations were performed by using the Sander module of Amber11.³⁹ MD simulations were performed also for the purpose of making the EL-2 more reasonably packed on the extracellular surface of the complex structure. The whole system was gradually heated to 300 K by a weak-coupling method⁴³ and equilibrated for about 2.0 ns. Throughout the MD simulations, a 10 Å nonbonded interaction cutoff was used and the nonbonded list was updated every 25 steps. The particle mesh Ewald (PME) method⁴⁴ was applied to treat long-range electrostatic interactions. The lengths of covalent bonds involving

hydrogen atoms were fixed with the SHAKE algorithm,⁴⁵ enabling the use of a 2-fs time step to numerically integrate the equations of motion. Finally, the production MD was kept running about 4.0 ns with a periodic boundary condition in the NTP ensemble at $T = 300$ K with Berendsen temperature coupling and at $P = 1$ atm with anisotropic molecule-based scaling.⁴³

Calculation of Binding Free Energy Change. We employed a molecular mechanics-Poisson–Boltzmann surface area (MM-PBSA) method⁴⁶ to estimate the binding free energy change from one inhibitor to another for the same receptor. According to the MM-PBSA method, the free energy of a ligand binding with the M5 receptor, ΔG_{bind} , is calculated from the difference between the free energy of the receptor–ligand complex ($G_{\text{R-L}}$) and the sum of the free energies of the unbound receptor (G_{R}) and ligand (G_{L}) as eq 1:

$$\Delta G_{\text{bind}} = G_{\text{R-L}} - (G_{\text{R}} + G_{\text{L}}) \quad (1)$$

ΔG_{bind} was evaluated as the sum of the changes in the MM gas-phase binding energy (ΔE_{MM}), solvation free energy (ΔG_{solv}), and entropic contribution ($-T\Delta S$).

$$\Delta G_{\text{bind}} = \Delta E_{\text{bind}} - T\Delta S \quad (2)$$

$$\Delta E_{\text{bind}} = \Delta E_{\text{MM}} + \Delta G_{\text{solv}} \quad (3)$$

$$\Delta G_{\text{solv}} = \Delta G_{\text{PB}} + \Delta G_{\text{np}} \quad (4)$$

$$\Delta G_{\text{np}} = \gamma \text{SASA} + \beta \quad (5)$$

The MM binding energies were calculated with the Sander module of the Amber program. Electrostatic solvation free energy (ΔG_{PB}) was calculated by the finite-difference solution to the Poisson–Boltzmann (PB) equation implemented in the Delphi program.^{47,48} The MSMS program⁴⁹ was used to calculate the solvent-accessible surface area (SASA) for the estimation of the nonpolar solvation energy (ΔG_{np}) using eq 5 with parameters $\gamma = 0.00542$ kcal/Å² and $\beta = 0.92$ kcal/mol.

The entropic contribution, $-T\Delta S$, to the binding free energy was calculated using a local program (a stand-alone program) developed in our own laboratory. The computational procedure used to evaluate the $-T\Delta S$ was the same as that described in our recent publications.^{50–53} As we described previously, the entropy contribution is divided into two parts: solvation entropy (ΔS_{solv}) and conformational entropy (ΔS_{conf}):

$$\Delta S = \Delta S_{\text{solv}} + \Delta S_{\text{conf}} \quad (6)$$

The solvation entropy is gained by solvent water molecules upon being displaced from the active site by the ligand during binding and was calculated by using the parameters established previously.⁵⁴ The contribution to the binding free energy from the conformational entropy change is proportional to the number (ΔN_{rot}) of the lost rotatable bonds during the binding:

$$-T\Delta S_{\text{conf}} = w(\Delta N_{\text{rot}}) \quad (7)$$

in which w is the scaling factor which may be slightly different for different receptors. Nevertheless, our previous studies^{50–53} consistently revealed that $w = 0.6434$ (the smallest value) to 0.8452 (the largest value). In the present study, we simply used the middle value of the range, i.e., $w = 0.7434 \pm 0.1009$, as the final result is not very sensitive to the w value within the range of the w values (see below).

It has been demonstrated⁵⁵ that the MM-PBSA method is reliable for calculating the relative binding free energies between various ligands with a same receptor via eq 8, although it might

not be very accurate for calculating the absolute binding free energies with a membrane protein.

$$\Delta\Delta G_{\text{bind}} = \Delta\Delta E_{\text{bind}} - T\Delta\Delta S \quad (8)$$

Most of the MD simulations were performed on a supercomputer (i.e., the Dell X-series Cluster with 384 nodes or 4768 processors) at University of Kentucky Center for Computational Sciences. Some other modeling and computations were carried out on SGI Fuel workstations in our own lab.

RESULTS AND DISCUSSION

Structural Model of M5 mAChR. The amino acid sequence alignment (Figure 1) between human M5 mAChR and turkey β_1 -AR shows that eight regions with high homology can be assigned to eight α -helices. These include the seven transmembrane helices (TM1 to TM7) and a small α -helix H8 consisting of residues Asn498 to Cys512, which is supposed to locate on the membrane cytoplasm interface. The finally obtained sequence alignment is depicted in Figure 1. Our structural model of M5 mAChR based on the sequence alignment depicted in Figure 1 is significantly different from the previously reported M5 mAChR model.^{31,33,34} For example, the start and the end positions of each TM in our current model are different from the corresponding positions in the previous reported M5 mAChR model³¹ using the crystal structure of rhodopsin as the template.²² In particular, the TM3 consists of 35 residues in our model, but it only consists of 21 residues in the previously reported model.³¹ On the basis of the reported crystal structures of class-A GPCRs,^{18,19,25–30} the TM3 was significantly longer than that of rhodopsin.^{22,24} This information supports our new model developed by using turkey β_1 -AR as the template and the sequence alignment depicted in Figure 1.

As modeled, the assembly of these helices in a lipid bilayer environment (Figure 2) is structurally organized similar to the template β_1 -AR.²⁸ The area per lipid (A_{L}) in the lipid bilayer was estimated to be ~ 63.1 Å², which is very close to that (~ 63.0 Å²) of the most commonly used POPC lipid bilayers described in the literature.⁵⁶ To track how M5 mAChR interacted with the surrounding lipid molecules, we counted the total number of contacts (N_{contact}) between the non-hydrogen atoms of the lipid bilayers and the non-hydrogen atoms of the M5 receptor for each snapshot of the MD trajectory. The criterion (cutoff) for the interatomic contact was set as 5.0 Å, and the tracked results are provided in Supporting Information (Figure S1). The tracked N_{contact} increased slightly during the first 2.0 ns of the MD simulation on the lipid molecules and fluctuated during the next 2.0 ns (the equilibration stage) of the MD simulation for the M5 mAChR–antagonist complex structure (see below for further discussion). The tracked N_{contact} remained constant, with an average N_{contact} value of 1019, during the final 4.0 ns of the MD simulation for the production stage (see below for further discussion). The changes of N_{contact} along the MD trajectory (Figure S1) suggest that the packing between the lipid molecules and the M5 mAChR was gradually improved and equilibrated during the MD simulation. The whole model of M5 mAChR appears to be in a conformation opening toward the extracellular side. The energy-minimized M5 mAChR structure (Figure 2) has a positional root-mean-square deviation (rmsd) of 0.23 Å for C α atoms from the initial structural model. Relative to the template β_1 -AR structure,²⁸ the rmsd for C α atoms of the seven TMs was only 0.52 Å. These small structural deviations suggest a high fidelity for the

of aromatic residues locates close to the extracellular end of TM6 and TM7 and is formed by residues Phe451, Trp455, Tyr458, Trp477, Tyr481, and Tyr485 (Figure 2D). These residues are stacked in parallel, while all the hydroxyl groups of residues Tyr458, Tyr481, and Tyr485 point to the internal cavity among TM2, TM3, TM5, TM6, and TM7. Residues Phe502, Phe506, and Leu509 from H8 interact with the hydrophobic residues Leu50 and Val57 from TM1, and Leu61 from IL-1 (Figure 2E), making H8 closely packed with the neighboring TM1 and the surrounding lipid molecules. Such specific local interactions must help to stabilize the whole receptor in the membrane environment. The X-ray structure of β_1 -AR²⁸ showed that its EL-2 formed a short α -helix and defined the entrance of the ligand-binding pocket. Unlike the EL-2 of β_1 -AR, the EL-2 of M5 mAChR cannot form any regular secondary structure, indicating that this loop might be easy to adapt to the outside stimulations.

Our energy-minimized M5 mAChR model is considerably different from the previously reported M5 mAChR models.^{31–34} The major difference exists not only in the starting position and the length of each helix but also in the assembly of the seven TMs. These differences between our current model and the previous models are mainly due to the fact that the more reasonable template²⁸ was used in our M5 mAChR structure modeling. As noted above, the template (i.e., the structure of β_1 -AR) used to build our model is phylogenetically closer to mAChRs, whereas the previous models^{31–34} were constructed based on the crystal structure of phylogenetically distant bovine rhodopsin.²² Histidine-substitution studies on M1 mAChR²⁰ revealed that the triple mutations such as Leu116His/Phe374His/Asn414His (the M1 numbering, and the same thereafter for residues of M1 mAChR) or Leu116His/Ser120His/Phe374His or Phe374His/Asn414His/Tyr418His led to high-affinity binding of the inactive receptor with Zn^{2+} ion, suggesting that these residues formed a network of intramolecular interactions. As these residues are highly conserved not only in mAChRs but also throughout the class-A GPCRs,^{17,23} it is reasonable to assume that the M5 mAChR also retains this network of intramolecular interactions. Comparing the sequence of the M5 receptor with that of M1 mAChR, residues Leu121 and Ser125 from TM3, Phe451 from TM6, and Asn491 and Tyr495 from TM7 of M5 mAChR are at the corresponding positions of those residues in M1 mAChR. A careful inspection of the structural model of M5 mAChR in the present study revealed that the side chains of these residues all point to the central cavity between TM3, TM5, TM6, and TM7 (Figure 2F). The distances among the C α atoms of residues Leu121, Ser125, and Phe451 are all close to 11.0 Å (Figure 2F, blue colored lines). Similar distances were found for the C α atoms among the triple residues Leu121-Phe451-Asn491 (Figure 2F, cyan colored lines) and the triple residues Phe451-Asn491-Tyr495 (Figure 2F, magenta colored lines). As observed in our M5 mAChR model structure, the side chains of these triple residues would approach each other inside the central cavity if they were mutated to the residue histidine. A Zn^{2+} -binding site will be formed by the side chains of any of these triple residues after possible local conformational adjustment, and the whole receptor structure will probably remain inactive. The usage of a better structural template²⁸ and the qualitative consistency with the observations of histidine-substitution studies²⁰ have made our current M5 mAChR structural model more reliable than the previously reported M5 mAChR models.^{31–34}

Binding Mode of M5 mAChR with Antagonists. The antagonist-binding site in M5 mAChR is located near the extracellular end of TM3, TM5, TM6, and TM7. As shown in Figure 3, TM2 and TM4 are also partially involved in the formation of the

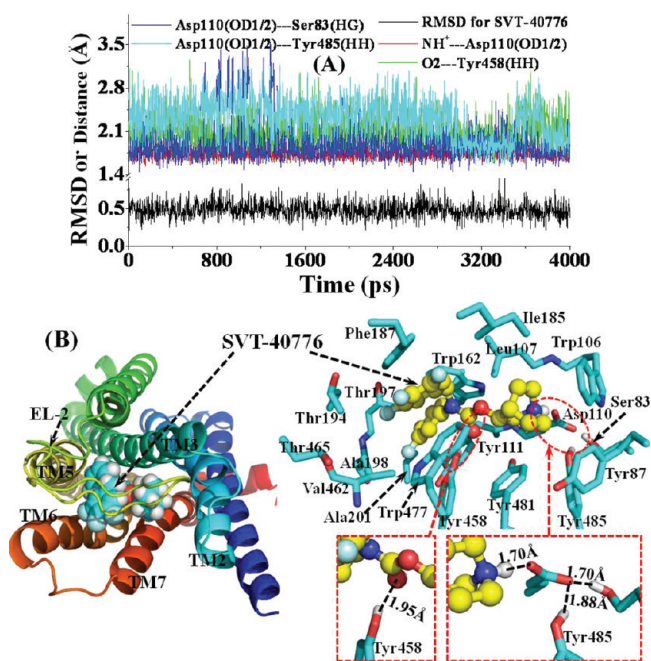


Figure 3. (A) Tracked positional rmsd for SVT-40776 from its original coordinates and tracked distances along the MD trajectory. $\text{NH}^+ \cdots \text{Asp110}(\text{OD1/2})$ represents the shortest distance between the proton at the cationic head of SVT-40776 and the negatively charged atoms (OD1 or OD2) on the side chain of residue Asp110. $\text{O2} \cdots \text{Tyr458}(\text{HH})$ is the distance for the hydrogen bond formed by the carbonyl oxygen of SVT-40776 with the Tyr458 side chain. $\text{Asp110}(\text{OD1/2}) \cdots \text{Ser83}(\text{HG})$ represents the distance for the hydrogen bond formed by the Asp110 side chain and the Ser83 side chain. $\text{Asp110}(\text{OD1/2}) \cdots \text{Tyr485}(\text{HH})$ is the distance for the hydrogen bond formed by the Asp110 side chain and the Tyr485 side chain. (B) Top view of representative structure for M5 mAChR–SVT-40776 complex, taken from the last snapshot of the MD simulation. The coloring scheme for the complex structure is the same as that used in Figure 2B, and SVT-40776 is shown as spheres (left panel) or ball-and-stick (right panel). Residues within 5 Å of SVT-40776 are labeled and shown in stick. The hydrogen-bonding interaction between the Asp110 side chain and the cationic head of SVT-40776, the hydrogen-bonding interaction between the carbonyl oxygen of SVT-40776 and the Tyr458 side chain, and the hydrogen-bonding interactions among side chains of Asp110, Ser83, and Tyr485 are shown in dashed lines along with the labeled distances.

antagonist-binding site. In addition, the antagonist-binding site is partially covered by EL-2. In a typical structure of the MD-simulated M5 mAChR–SVT-40776 complex (Figure 3B) at the snapshot of the MD trajectory at 4.0 ns (Figure 3A), the SVT-40776 molecule is oriented horizontally inside the binding pocket (Figure 3B). The cationic head of SVT-40776 is anchored around the negatively charged side chain of residue Asp110 from TM3, interacting with each other through electrostatic attraction and strong hydrogen bonding (Figure 3B). As tracked from the MD simulations (Figure 3A), the average shortest distance for the hydrogen bond through the proton at the cationic head of SVT-40776 and the negatively charged atoms at the side chain of Asp110 is 1.75 Å. Meanwhile, residue Asp110 is also hydrogen bonded with the side chain of Ser83 from TM2 (blue curve in Figure 3A) and the side chain of Tyr485 from TM7 (cyan curve in Figure 3A). The cationic head of SVT-40776 is also closely packed with residues Trp106 and Leu107 from TM3, Tyr481 from TM7, and Ile185 from EL-2. Residue Tyr87 from TM2 is also within 5 Å from the cationic head of SVT-40776.

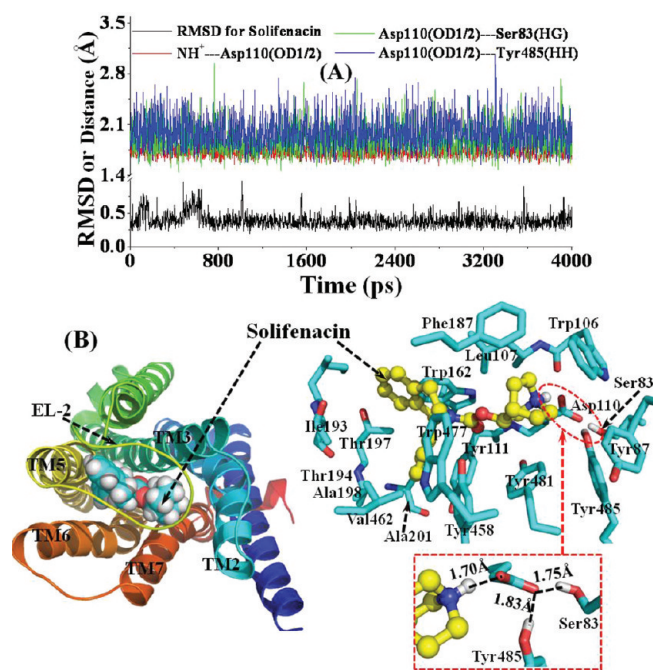


Figure 4. (A) Plots of the tracked positional rmsd for solifenacin from its original coordinates and tracked distances. $\text{NH}^+ \cdots \text{Asp110}(\text{OD1/2})$ represents the shortest distance between the proton at the cationic head of solifenacin and the negatively charged atoms (OD1 or OD2) on the side chain of residue Asp110. $\text{Asp110}(\text{OD1/2}) \cdots \text{Ser83}(\text{HG})$ represents the distance for the hydrogen bond formed by the Asp110 side chain and the Ser83 side chain. $\text{Asp110}(\text{OD1/2}) \cdots \text{Tyr485}(\text{HH})$ is the distance for the hydrogen bond formed by the Asp110 side chain and the Tyr485 side chain. (B) Top view of representative structure for M5 mAChR-solifenacin complex, taken from the last snapshot of the MD simulations. The coloring scheme for the complex structure is the same as that used in Figure 2B, and the solifenacin is presented as spheres (left panel) or ball-and-stick (right panel). Residues within 5 Å of solifenacin are labeled and shown in stick. The hydrogen-bonding interaction between the Asp110 side chain and the cationic head of solifenacin and the hydrogen-bonding interactions among side chains of Asp110, Ser83, and Tyr485 are shown in dashed lines along with the labeled distances.

The carbonyl oxygen of SVT-40776 is always hydrogen bonded with the hydroxyl group on the side chain of Tyr458 from TM6 with an average distance of 2.08 Å throughout all the MD simulations (green curve of Figure 3A). One of the fluoro-substituted phenyl groups of SVT-40776 is packed in parallel with the underneath Tyr111 from TM3 and the above Phe187 from EL-2. It is also packed perpendicularly with the side chain of Trp162 from TM4. This fluoro-substituted phenyl group of SVT-40776 is also surrounded by residues Thr194, Thr197, Ala198, and Ala201 from TM5. The fluorine atom at the meta-position of the phenyl group of SVT-40776 has no specific hydrogen-bonding interaction with the surrounding residues as observed from the MD-simulated complex structure (Figure 3B). However, the three fluoro substitutions on another phenyl group of SVT-40776 are all solvent-exposed, probably hydrogen bonding with surrounding water molecules. One of these three fluoro substitutions is also close to the side chain of Ser465 from TM6, but without direct contact, indicating that they interact indirectly through water molecules. In addition, the three fluoro-substituted phenyl groups of SVT-40776 are packed in parallel with the aromatic side chain of residue Trp477 from TM7 and Phe187 from EL-2.

The residue Asp110 is totally conserved across all subtypes of mAChRs. The same Asp residue at a similar position in M1 and M2 mAChRs has been indicated to play a vital role in the binding of agonist acetylcholine by Asp/Glu mutation.¹¹ Residues Tyr111, Tyr458, Tyr481, and Tyr485 are also conserved for mAChRs, and the residues at the corresponding positions in M3 mAChR were found to be important for the binding of agonists studied by cross-linking strategy.⁵⁷ It would be interesting to design further biological studies including site-directed mutagenesis in the future to verify the computationally predicted binding mode of SVT-40776 in this study.

Figure 4 depicts the tracked important distances concerning the intermolecular interactions in the MD-simulated structural model of M5 mAChR-solifenacin complex. The mode of binding of solifenacin with M5 mAChR is generally similar to that of SVT-40776 (Figure 3). The detailed atomic interactions between solifenacin and M5 mAChR are featured as electrostatic, hydrogen-bonding, and hydrophobic contacts, as shown in Figure 4 for a typical structure of the MD-simulated complex at the 4.0 ns snapshot. The proton at the cationic head of solifenacin is also hydrogen bonded with the side chain of Asp110 with an average distance of 1.75 Å during the MD simulation (Figure 4A). For a major difference between the M5 mAChR-solifenacin binding and the M5 mAChR-SVT-40776 binding, Phe187 is packed with the cationic headgroup of solifenacin, whereas Ile185 is packed with the cationic headgroup of SVT-40776. For another significant difference, there is no hydrogen-bonding interaction between the carbonyl oxygen of solifenacin and the surrounding residues including Tyr458 (Figure 4B), whereas a persistent hydrogen bond is formed between the carbonyl oxygen of SVT-40776 and the side chain of Tyr458 (Figure 3). This key structural difference in intermolecular interactions may be helpful to understand why the binding affinity of SVT-40776 is much higher than that of solifenacin with the same receptor. As measured,^{13,15} the dissociation constant (K_d) of solifenacin with M5 mAChR was 31 nM and the K_d of SVT-40776 was 0.4 nM. The phenyl group on the tail of solifenacin is located at a subsite similar to that of SVT-40776, and the tail of solifenacin is loosely packed with the side chains of residues Val462 and Trp477.

For a better understanding of the binding affinity difference between solifenacin and SVT-40776, the MM-PBSA calculations were performed to estimate the binding free energy change, i.e., $\Delta\Delta G_{\text{bind}}$ in eq 8, from solifenacin to SVT-40776 for the binding with M5 mAChR by using the energy-minimized receptor-ligand binding structures depicted in Figures 3 and 4. On the basis of the MM-PBSA calculations, we obtained $\Delta\Delta E_{\text{bind}} = -1.4$ kcal/mol and $-T\Delta\Delta S = -0.9 \pm 0.3$ kcal/mol corresponding to $w = 0.7434 \pm 0.1009$. These data suggest that both the enthalpy and entropy favor SVT-40776 binding with the receptor. Thus, according to eq 8, the MM-PBSA calculations led to the computational prediction of $\Delta\Delta G_{\text{bind}} = -2.3 \pm 0.3$ kcal/mol. For comparison, we may also convert the experimentally measured dissociation constant ($K_d = [\text{R}][\text{L}]/[\text{R-L}]$) to the binding free energy, denoted by $\Delta G_{\text{bind}}(\text{expt})$, by using the well-known thermodynamic equation, i.e., $\Delta G_{\text{bind}} = RT \ln K_d$ at $T = 298.15$ K. On the basis of the experimental data, i.e., $K_d = 0.4$ nM for SVT-40776 and $K_d = 31$ nM for solifenacin,^{13,15} we have $\Delta\Delta G_{\text{bind}}(\text{expt}) = RT \ln K_d(\text{SVT-40776}) - RT \ln K_d(\text{solifenacin}) = -2.58$ kcal/mol. Our computationally estimated $\Delta\Delta G_{\text{bind}}$ value of -2.3 ± 0.3 kcal/mol is in good agreement with the experimentally derived $\Delta\Delta G_{\text{bind}}(\text{expt})$ value of -2.58 kcal/mol. The good agreement between the computational and experimental

binding free energy differences suggests that the modeled complex structures for M5 mAChR binding with the antagonists are reliable.

CONCLUSIONS

The present computational modeling, molecular docking, and molecular dynamics simulations have led us to develop a reasonable 3D structural model of M5 mAChR and understand its binding with antagonists SVT-40776 and solifenacin. Our modeled 3D structures of M5 mAChR in complex with the antagonists have provided valuable structural insights concerning M5 mAChR interaction with antagonists at the atomic level. In common, the cationic headgroup of both antagonists interacts with residue Asp110 from TM3 through electrostatic attraction and hydrogen bonding, and the cationic head is also packed tightly with the surrounding aromatic residues from TM3 and TM7. However, the carbonyl oxygen of SVT-40776 is persistently hydrogen bonded with residue Tyr458, whereas there is no hydrogen-bonding interaction between the carbonyl oxygen of solifenacin and the surrounding residues. This significant difference in intermolecular interactions contributes to the observed difference in the binding affinity between these two antagonists with the same receptor. The good agreement between the calculated binding free energy change (-2.3 ± 0.3 kcal/mol) from solifenacin to SVT-40776 and the experimentally derived binding free energy change (-2.58 kcal/mol) suggests that our modeled M5 mAChR structure and its complexes with the antagonists are reliable. The new structural insights obtained from this computational study should be valuable for the design of further biochemical and pharmacological studies on the detailed structures of M5 and other subtypes of mAChRs.

ASSOCIATED CONTENT

S Supporting Information. Additional figure (Figure S1) for the tracked number of contacts between M5 mAChR and the surrounding lipid bilayer molecules. This material is available free of charge via the Internet at <http://pubs.acs.org>.

AUTHOR INFORMATION

Corresponding Author

*Tel: 859-323-3943. Fax: 859-323-3575. E-mail: zhan@uky.edu.

ACKNOWLEDGMENT

This work was supported by NIH (DA025948 and DA030667). The authors also acknowledge the Center for Computational Sciences (CCS) at the University of Kentucky for supercomputing time on a Dell Supercomputer Cluster consisting of 388 nodes or 4816 processors.

REFERENCES

- (1) Bonner, T. I.; Young, A. C.; Brann, M. R.; Buckley, N. J. Cloning and expression of the human and rat m5 muscarinic acetylcholine receptor genes. *Neuron* **1988**, *1*, 403–410.
- (2) Eglen, R. M.; Choppin, A.; Dillon, M. P.; Hegde, S. Muscarinic receptor ligands and their therapeutic potential. *Curr. Opin. Chem. Biol.* **1999**, *3*, 426–432.
- (3) Bymaster, F. P.; McKinzie, D. L.; Felder, C. C.; Wess, J. Use of M₁-M₅ muscarinic receptor knockout mice as novel tools to delineate

the physiological roles of the muscarinic cholinergic system. *Neurochem. Res.* **2003**, *28*, 437–442.

- (4) Jonkam, C.; Zhu, Y.; Jacob, S.; Rehberg, S.; Kraft, E.; Hamahata, A.; Nakano, Y.; Traber, L. D.; Herndon, D. N.; Traber, D. L.; Hawkins, H. K.; Enkhbaatar, P.; Cox, R. A. Muscarinic receptor antagonist therapy improve acute pulmonary dysfunction after smoke inhalation injury in sheep. *Crit. Care Med.* **2010**, *38*, 2339–2344.

- (5) Yeomans, J.; Forster, G.; Blaha, C. M₅ muscarinic receptors are needed for slow activation of dopamine neurons and for rewarding brain stimulation. *Life Sci.* **2001**, *68*, 2449–2456.

- (6) Forster, G. L.; Yeomans, J. S.; Takeuchi, J.; Blaha, C. D. M₅ muscarinic receptors are required for prolonged accumbal dopamine release after electrical stimulation of the pons in mice. *J. Neurosci.* **2002**, *22*, RC190.

- (7) Bendor, J.; Lizardi-Ortiz, J.; Westphalen, R. I.; Hemmings, H. C., Jr. Sulzer, D.; Flajolet, M.; Greengard, P. AGAP1/AP-3-dependent endocytic recycling of M₅ muscarinic receptors promotes dopamine release. *EMBO J.* **2010**, *29*, 2813–2826.

- (8) Araya, R.; Noguchi, T.; Yuhki, M.; Kitamura, N.; Higuchi, M.; Saïdo, T. C.; Seki, K.; Itohara, S.; Kawano, M.; Tanemura, K.; Wess, J.; Yamada, M. Loss of M₅ muscarinic acetylcholine receptors leads to cerebrovascular and neuronal abnormalities and cognitive deficits in mice. *Neurobiol. Dis.* **2006**, *24*, 334–344.

- (9) Steidl, S.; Yeomans, J. S. M₅ muscarinic receptor knockout mice show reduced morphine-induced locomotion but increased locomotion after cholinergic antagonism in the ventral tegmental area. *J. Pharm. Exp. Ther.* **2009**, *328*, 263–275.

- (10) Raffa, R. B. The M₅ muscarinic receptor as possible target for treatment of drug abuse. *J. Clin. Pharm. Ther.* **2009**, *34*, 623–629.

- (11) Hulme, E.; Curtis, C. A. M.; Page, K. M.; Jones, P. G. The role of charge interactions in muscarinic agonist binding, and receptor-response coupling. *Life Sci.* **1995**, *56*, 891–898.

- (12) Gridges, T. M.; Marlo, J. E.; Niswender, C. M.; Jones, C. K.; Jadhav, S. B.; Gentry, P. R.; Plumley, H. C.; Weaver, C. D.; Conn, P. J.; Lindsley, C. W. Discovery of the first highly M₅-preferring muscarinic acetylcholine receptor ligand, an M₅ positive allosteric modulator derived from a series of 5-trifluoromethoxy N-benzyl isatins. *J. Med. Chem.* **2009**, *52*, 3445–3448.

- (13) Ohtake, A.; Saitoh, C.; Yuyanma, H.; Ukai, M.; Okutsu, H.; Noguchi, Y.; Hatanaka, T.; Suzuki, M.; Sasamata, M.; Miyata, K. Pharmacological characterization of a new antimuscarinic agent, sulifenacin succinate, in comparison with other antimuscarinic agents. *Biol. Pharm. Bull.* **2007**, *30*, 54–58.

- (14) Jones, L. H.; Randall, A.; Napier, C.; Trevethick, M.; Sreckovic, S.; Watson, J. Design and synthesis of a fluorescent muscarinic antagonist. *Bioorg. Med. Chem. Lett.* **2008**, *18*, 825–827.

- (15) Salcedo, S.; Davalillo, S.; Cabellos, J.; Lagunas, C.; Balsa, D.; Pérez-del-Pulgar, S.; Ballarín, M.; Fernández, A. G. *In vivo* and *in vitro* pharmacological characterization of SVT-40776, a novel M₃ muscarinic receptor antagonist, for the treatment of overactive bladder. *Br. J. Pharmacol. Soc.* **2009**, *156*, 807–817.

- (16) Casarosa, P.; Bouyssou, T.; Germeyer, S.; Schnapp, A.; Gantner, F.; Pieper, M. Preclinical evaluation of long-acting muscarinic antagonists: comparison of tiotropium and investigational drugs. *J. Pharmacol. Exp. Ther.* **2009**, *330*, 660–668.

- (17) Congreve, M.; Langmead, C. J.; Mason, J. S.; Marshall, F. H. Progress in structure based drug design for G protein-coupled receptors. *J. Med. Chem.* **2011**, *54*, 4283–4311.

- (18) Jaakola, V.-P.; Ijzerman, A. P. The crystallographic structure of the human adenosine A_{2A} receptor in a high-affinity antagonist-bound state: implications for GPCR drug screening and design. *Curr. Opin. Struct. Biol.* **2010**, *20*, 401–414.

- (19) Shukla, A. K.; Sun, J.-P.; Lefkowitz, R. J. Crystallizing thinking about the β_2 -adrenergic receptor. *Mol. Pharmacol.* **2008**, *73*, 1333–1338.

- (20) Lu, Z.-L.; Hulme, E. C. A network of conserved intramolecular contacts defines the off-state of the transmembrane switch mechanism in a seven-transmembrane receptor. *J. Biol. Chem.* **2000**, *275*, 5682–5686.

- (21) Bokoch, M. P.; Zou, Y.; Rasmussen, S. G. F.; Liu, C. W.; Nygaard, R.; Rosenbaum, D. M.; Fung, J. J.; Choi, H.-J.; Thian, F. S.;

Kobilka, T. S.; Puglisi, J. D.; Weis, W. I.; Pardo, L.; Prosser, R. S.; Mueller, L.; Kobilka, B. K. Ligand-specific regulation of the extracellular surface of a G-protein coupled receptor. *Nature* **2010**, *463*, 108–114.

(22) Palczewski, K.; Kumazawa, T.; Hori, T.; Behnke, C. A.; Motoshima, H.; Fox, B. A.; Trong, I. L.; Teller, D. C.; Okada, T.; Stenkamp, R. E.; Yamamoto, M.; Miyano, M. Crystal structure of rhodopsin: a G protein-coupled receptor. *Science* **2000**, *289*, 739–745.

(23) Mustafa, D.; Palczewski, K. Topology of class A G protein-coupled receptors: insights gained from crystal structures of rhodopsins, adrenergic and adenosine receptors. *Mol. Pharmacol.* **2009**, *75*, 1–12.

(24) Angel, T. E.; Chance, M. R.; Palczewski, K. Conserved waters mediate structural and functional activation of family A (rhodopsin-like) G protein-coupled receptors. *Proc. Natl. Acad. Sci. U.S.A.* **2009**, *106*, 8555–8560.

(25) Rasmussen, S. G. F.; Choi, H.-J.; Rosenbaum, D. M.; Kobilka, T. S.; Thian, F. S.; Edwards, P. C.; Burghammer, M.; Ratnala, V. R. P.; Sanishvili, R.; Fischetti, R. F.; Schertler, G. F. X.; Weis, W. I.; Kobilka, B. K. Crystal structure of the human β_2 adrenergic G-protein-coupled receptor. *Nature* **2007**, *450*, 383–388.

(26) Cherezov, V.; Rosenbaum, D. M.; Hanson, M. A.; Rasmussen, S. G. F.; Thian, F. S.; Kobilka, T. S.; Choi, H.-J.; Kuhn, P.; Weis, W. I.; Kobilka, B. K.; Stevens, R. C. High-resolution crystal structure of an engineered human β_2 -adrenergic G protein-coupled receptor. *Science* **2007**, *318*, 1258–1265.

(27) Hanson, M. A.; Cherezov, V.; Griffith, M. T.; Roth, C. B.; Jaakola, V.-P.; Chien, E. Y. T.; Velasquez, J.; Kuhn, P.; Stevens, R. G. A specific cholesterol binding site is established by the 2.8 Å structure of the human β_2 -adrenergic receptor. *Structure* **2008**, *16*, 897–905.

(28) Warne, T.; Serrano-Vega, M. J.; Baker, J. G.; Moukhametzianov, R.; Edwards, P. C.; Henderson, R.; Leslie, A. G. W.; Tate, C. G.; Schertler, G. F. Structure of a β_1 -adrenergic G-protein-coupled receptor. *Nature* **2008**, *454*, 486–492.

(29) Jaakola, V.-P.; Griffith, M. T.; Hanson, M. A.; Cherezov, V.; Chien, E. Y. T.; Lane, J. R.; Ijzerman, A. P.; Stevens, R. C. The 2.6 angstrom crystal structure of a human A_{2A} adenosine receptor bound to an antagonist. *Science* **2008**, *322*, 1211–1217.

(30) Wu, B.; Chien, E. Y.; Mol, C. D.; Fenalti, G.; Liu, W.; Katritch, V.; Abagyan, R.; Brooun, A.; Wells, P.; Bi, F. C.; Hamel, D. J.; Kuhn, P.; Handel, T. M.; Cherezov, V.; Stevens, R. C. Structures of the CXCR4 chemokine GPCR with small-molecule and cyclic peptide antagonists. *Science* **2010**, *330*, 1066–1071.

(31) Pedretti, A.; Vistoli, G.; Marconi, C.; Testa, B. Muscarinic receptors: a comparative analysis of structural features and binding modes through homology modeling and molecular docking. *Chem. Biodiversity* **2006**, *3*, 481–501.

(32) Avlani, V. A.; Gregory, K. J.; Morton, C. J.; Parker, M. W.; Sexton, P. M.; Christopoulos, A. Critical role for the second extracellular loop in the binding of both orthosteric and allosteric G protein-coupled receptor ligands. *J. Biol. Chem.* **2007**, *282*, 25677–25686.

(33) Peng, J. Y.-C.; Vaidehi, N.; Hall, S. E.; Goddard, W. A., III. The predicted 3D structures of the human M_1 muscarinic acetylcholine receptor with agonist or antagonist bound. *ChemMedChem* **2006**, *1*, 878–890.

(34) Vistoli, G.; Pedretti, A.; Dei, S.; Scapecchi, S.; Marconi, C.; Romanelli, M. N. Docking analyses on human muscarinic receptors: Unveiling the subtypes peculiarities in agonist binding. *Bioorg. Med. Chem.* **2008**, *16*, 3049–3058.

(35) Thompson, J. D.; Higgins, D. G.; Gibson, T. J. CLUSTAL W: improving the sensitivity of progressive multiple sequence alignment through sequence weighting, position-specific gap penalties, and weight matrix choice. *Nucleic Acids Res.* **1994**, *22*, 4673–4680.

(36) Henikoff, S.; Henikoff, J. G. Amino-acid substitution matrices from protein blocks. *Proc. Natl. Acad. Sci. USA.* **1992**, *89*, 10915–10919.

(37) Humphrey, W.; Dalke, A.; Schulten, K. VMD-Visual Molecular Dynamics. *J. Mol. Graphics* **1996**, *14*, 33–38.

(38) Frisch, M. J.; Trucks, G. W.; Schlegel, H. B.; Scuseria, G. E.; Robb, M. A.; Cheeseman, J. R.; Montgomery, J. A., Jr.; Vreven, T.; Kudin, K. N.; Burant, J. C.; Millam, J. M.; Iyengar, S. S.; Tomasi, J.; Barone, V.; Mennucci, B.; Cossi, M.; Scalmani, G.; Rega, N.; Petersson, G. A.

Nakatsuji, H.; Hada, M.; Ehara, M.; Toyota, K.; Fukuda, R.; Hasegawa, J.; Ishida, M.; Nakajima, T.; Honda, Y.; Kitao, O.; Nakai, H.; Klene, M.; Li, X.; Knox, J. E.; Hratchian, H. P.; Cross, J. B.; Adamo, C.; Jaramillo, J.; Gomperts, R.; Stratmann, R. E.; Yazyev, O.; Austin, A. J.; Cammi, R.; Pomelli, C.; Ochterski, J. W.; Ayala, P. Y.; Morokuma, K.; Voth, G. A.; Salvador, P.; Dannenberg, J. J.; Zakrzewski, V. G.; Dapprich, S.; Daniels, A. D.; Strain, M. C.; Farkas, O.; Malick, D. K.; Rabuck, A. D.; Raghavachari, K.; Foresman, J. B.; Ortiz, J. V.; Cui, Q.; Baboul, A. G.; Clifford, S.; Cioslowski, J.; Stefanov, B. B.; Liu, G.; Liashenko, A.; Piskorz, P.; Komaromi, I.; Martin, R. L.; Fox, D. J.; Keith, T.; Al-Laham, M. A.; Peng, C. Y.; Nanayakkara, A.; Challacombe, M.; Gill, P. M. W.; Johnson, B.; Chen, W.; Wong, M. W.; Gonzalez, C.; Pople, J. A. *Gaussian 03, Revision A.1*, Gaussian, Inc., Pittsburgh, PA, 2003.

(39) Case, D. A.; Darden, T. A.; Cheatham, T. E., III; Simmerling, C. L.; Wang, J.; Duke, R. E.; Luo, L.; Walker, R. C.; Zhang, W.; Merz, K. M.; Roberts, B.; Wang, B.; Hayik, S.; Roitberg, A.; Seabra, G.; Kolosváry, I.; Wong, K. F.; Paesani, F.; Vanicek, J.; Liu, L.; Wu, X.; Brozell, S. R.; Steinbrecher, T.; Gohlke, H.; Cai, Q.; Ye, X.; Wang, J.; Hsieh, M.-J.; Cui, G.; Roe, D. R.; Mathews, D. H.; Seetin, M. G.; Sagui, C.; Babin, V.; Luchko, T.; Gusarov, S.; Kovalenko, A.; Kollman, P. A. *AMBER 11*, University of California, San Francisco, 2010.

(40) Jorgensen, W. L.; Chandrasekhar, J.; Madura, J. D.; Impey, R. W. Comparison of Simple Potential Functions for Simulating Liquid Water. *J. Chem. Phys.* **1983**, *79*, 926–935.

(41) Morris, G. M.; Goodsell, D. S.; Halliday, R. S.; Huey, R.; Hart, W. E.; Belew, R. K.; Olson, A. J. Automated docking using a Lamarckian genetic algorithm and empirical binding free energy function. *J. Comput. Chem.* **1998**, *19*, 1639–1662.

(42) Solis, F. J.; Wets, R. J. B. Minimization by random search techniques. *Math. Operations Res.* **1981**, *6*, 19–30.

(43) Berendsen, H. J. C.; Postma, J. P. M.; van Gunsteren, W. F.; DiNola, A.; Haak, J. R. Molecular dynamics with coupling to an external bath. *J. Chem. Phys.* **1984**, *81*, 3684–3690.

(44) Darden, T.; York, D.; Pedersen, L. Particle mesh Ewald—an Nlog(N) method for Ewald sums in large systems. *J. Chem. Phys.* **1993**, *98*, 10089–10092.

(45) Ryckaert, J. P.; Ciccotti, G.; Berendsen, H. J. C. Numerical integration of the Cartesian equations of motion of a system with constraints: Molecular dynamics of n-alkanes. *J. Comput. Phys.* **1977**, *23*, 327–341.

(46) Kollman, P. A.; Massova, I.; Reyes, C.; Kuhn, B.; Huo, S.; Chong, L.; Lee, M.; Lee, T.; Duan, Y.; Wang, W.; Donini, O.; Cieplak, P.; Srinivasan, J.; Case, D. A.; Cheatham, T. E. Calculating Structures and Free Energies of Complex Molecules: Combining Molecular Mechanics and Continuum Models. *Acc. Chem. Res.* **2000**, *33*, 889–897.

(47) Gilson, M. K.; Sharp, K. A.; Honig, B. H. Calculating electrostatic interactions in biomolecules: Method and error assessment. *J. Comput. Chem.* **1987**, *9*, 327–335.

(48) Jayaram, B.; Sharp, K. A.; Honig, B. The electrostatic potential of B-DNA. *Biopolymers* **1989**, *28*, 975–993.

(49) Sanner, M. F.; Olson, A. J.; Spehner, J.-C. Reduced surface: an efficient way to compute molecular surfaces. *Biopolymers* **1996**, *38*, 305–320.

(50) Pan, Y.; Gao, D.; Zhan, C.-G. Modeling the catalysis of anti-cocaine catalytic antibody: Competing reaction pathways and free energy barriers. *J. Am. Chem. Soc.* **2008**, *130*, 5140–5149.

(51) Lu, H.; Goren, A. C.; Zhan, C.-G. Characterization of the structures of phosphodiesterase 10 binding with adenosine 3',5'-monophosphate and guanosine 3',5'-monophosphate by hybrid quantum mechanical/molecular mechanical calculations. *J. Phys. Chem. B* **2010**, *114*, 7022–7028.

(52) Chen, X.; Zhan, X.; Xiong, Y.; Liu, J.; Zhan, C.-G. Fundamental reaction pathway and free energy profile for hydrolysis of intracellular second messenger adenosine 30,50-cyclic monophosphate (cAMP) catalyzed by phosphodiesterase-4. *J. Phys. Chem. B* **2011**, *115*, 12208–12219.

(53) Li, D.; Huang, X.; Han, K.; Zhan, C.-G. Catalytic mechanism of cytochrome P450 for 5'-hydroxylation of nicotine: fundamental reaction pathways and stereoselectivity. *J. Am. Chem. Soc.* **2011**, *133*, 7416–7427.

(54) Raha, K.; Merz, K. M. Large scale validation of a quantum mechanics based scoring function: Predicting the binding affinity and

the binding mode of a diverse set of protein–ligand complexes. *J. Med. Chem.* **2005**, *48*, 4558–4575.

(55) Huang, X.; Gu, H.-H.; Zhan, C.-G. Mechanism for cocaine blocking the transport of dopamine: insights from molecular modeling and dynamics simulations. *J. Phys. Chem.* **2009**, *113*, 15057–15066.

(56) Sapay, N.; Tieleman, D. P. Combination of the CHARMM27 force field with united-atom lipid force fields. *J. Comput. Chem.* **2011**, *32*, 1400–1410.

(57) Han, S.-J.; Hamdan, F. F.; Kim, S.-K.; Jacobson, K. A.; Bloodworth, L. M.; Li, B.; Wess, J. Identification of an agonist-induced conformational change occurring adjacent to the ligand-binding pocket of the M₃ muscarinic acetylcholine receptor. *J. Biol. Chem.* **2005**, *280*, 34849–34858.